In silico druggability analysis of Cdc37 in candidiasis

Sneha Dey[1], Sanjib Das[2]*, Amalesh Mondal[2,3], Deepanjan Chattopadhyay[2], Paromita Saha Mondal[2], Tanushree Mondal[2], Madhurima Roy[2], Tanima Saha[2]*

[1]Department of Bioscience, JIS University

[2]Department of Molecular Biology and Biotechnology, University of Kalyani

[3]Department of Physiology, Katwa College, Katwa, Purba Bardhaman, West Bengal, 713130, India

***Corresponding Author**

DOI: https://doi.org/10.51244/IJRSI.2026.1307000341

Received: 02 August 2026; Accepted: 07 August 2026; Published: 18 August 2026

ABSTRACT:

Candida albicans is an opportunistic fungal pathogen that participates in the life-threatening bloodstream infections. Although the virulent nature of the fungus has been well studied, targeting its druggability for therapeutics still requires extensive research. The special structural morphogenesis known as the hyphae leads to pathogenic biofilm formation by the organism. Pkc1 is the kinase protein involved in hyphae formation. Pkc1 is a client kinase that binds to the co-chaperone Cdc37. This Cdc37-Pkc1 complex then associates with the Hsp90 chaperone machinery. Together, Hsp90 and Cdc37 stabilize and activate the Pkc1 protein for proper cell integrity signalling. When Hsp90 loses control over Pkc1, the client protein participates in hyphal development through the CWI pathway. The main focus is on the interaction of Cdc37 and Pkc1; the Pkc1 protein binds to the N-terminal domain of Cdc37. Molecular docking studies of the Cdc37 protein with FDA-approved ligands targeting its N-terminal domain may inhibit the formation of the Cdc37–Pkc1 complex. Among the approved drugs we found that Nilotinib shows the best binding affinity towards the domain-specific inhibition of Cdc37.

Keywords: Candida albicans, Cdc37, Pkc1, Drug repurposing, Molecular docking

INTRODUCTION:

Candida albicans belonging to the class *Saccharomycetes*, is a pathogenic yeast commonly found in the human gut microbiome (Nobile and Johnson 2015). It is detected in about 40-60% individuals in the gastrointestinal tract and mouth of healthy adults (Ghannoum et al. 2010). Estimates by the NIH indicate that microbial biofilms account for over 80% of infections in the United States (Tsui et al. 2016). *C. albicans* causes the most frequent nosocomial infections accounting for approximately 50,000-60,000 cases every year in the USA alone (Mayer et al. 2013). It shows its virulence or pathogenic nature in immunocompromised individuals under different physiological conditions (Ciurea et al. 2020). The majority of diseases caused by this pathogen are associated with biofilm formation on host. Biofilm formation by this fungal organism leads to mortality rates up to 30% higher than localized yeast infections(Tsui et al. 2016). Due to the environmental factors, the species undergoes a rapid transition from yeast to hyphae (Sudbery 2011). Both the morphological forms are important, as both play a pivotal role in pathogenesis and survival, where yeast cells propagate through blood and the hyphal cells lead to the infection (Mayer et al. 2013). Relatively very few drugs successfully treat candidiasis, including, fluconazole, amphotericin B and clotrimazole (Spampinato and Leonardi 2013).

The druggability for the particular species is not much known, but the proteins responsible for the hyphae formation are widely collected and researched. Among them, Pkc1(Protein kinase C), a kinase protein of Hsp90 (Heat-Shock Protein 90) is involved in hyphal maturation through cell wall integrity pathway (CWI) (Xie et al. 2016). The pathway does include other proteins like Mkk2, Bck1 and Mkc1 (Robbins and Cowen 2023). Beside

this, Pkc1 also regulates the hyphal development by the Cyr1 dependent mechanisms (Robbins and Cowen 2023).

The CWI entails the MAP kinase cascade, Pkc1 needs a molecular chaperone protein to stabilize and activate it (Engler et al. 2026). The Hsp90 (Heat shock protein) and its co-chaperone Cdc37 comes to play. As a client protein, Pkc1 requires additional machinery to bind to the molecular chaperone protein, Hsp90, so cdc37, a co-chaperone acts as a molecular bridge to help bind the client protein and chaperone together (Robbins and Cowen 2023).

The co-chaperone, Cdc37, is a kinase specific protein which has a N- terminal binding site and may therefore be considered as a potential drug target for disease control. The client protein kinase binds to the N-terminal domain of Cdc37 establishing a stable client-Cdc37 binary complex (Keramisanou et al. 2016). In *C. albicans*, the protein not only stabilizes the client protein but also interacts with Hsp90 even under stress by high-connectivity interactors like Ckb1, which also affects the target kinases (Diezmann et al. 2012). Therefore, to disrupt the function of this ternary complex, we perform drug repositioning studies disrupting Cdc37 functioning.

METHODOLOGY:

Protein structure modelling

In the absence of a crystal structure, the homology-based modelling of the Cdc37protein was performed, to study the 3-D structure. The FASTA sequence of the Cdc37 protein was retrieved from Uniport (https://www.uniprot.org/) using the strain SC5314/ATCC MYA-2876 under entry name CDC37_CANAL (Bateman et al. 2023). The full 508-amino-acids was used for acquiring predicted structures of the protein. Comparative structure modeling was performed using Swiss-model server (Waterhouse et al. 2018). The server provided four model structures. The selection of the model was based on the GMQE score, higher GMQE score represents that the predicted structure is reliable and accurate (Biasini et al. 2014). The AlphaFold template-based model out of the four predicted structure was noted to have the highest GMQE score. Structure validation was performed with the selected model.

Structure Validation:

The modeled structure required validation to confirm its reliability for downstream applications. A validation for structure prevents hidden errors early, like the side chains overlapping, incorrect bond lengths and missing amino acid residues. The Saves v6.0 web server was used to verify the geometric feasibility and stereochemical quality of the predicted structure. Saves v6.0 checks the structure through 4 different program system- PROCHECK (especially for the Ramachandran Plot), ERRAT (for statistical excellence of non-covalent interactions), VERIFY3D (to analyze any packing issues of atoms) and WHATCHECK (to do extensive checking of the stereochemical criteria). For further validation ProSA, a diagnostic tool was used that evaluates the Z-score of the model(Wiederstein and Sippl 2007). The Z-score value shows the comprehensive performance of the protein model presenting its total energy. It also provides us with the energy plot of the residues, locating the faulty regions and a 3-D visualization of the whole protein including the faulty regions for further necessary refinements.

Drug screening:

After obtaining a validated structure of the Cdc37 protein, identification of the optimal binding pocket for Cdc37 and subsequently selection of the drugs targeting that pocket in the co-chaperone protein for further protein–ligand docking studies were performed. DrugRep server is a bioinformatics tool for both receptor-based and ligand-based screening, providing a 3-D image of the different pockets involved and enlisting the drugs ranking according to their score which shows their binding affinity (Gan et al. 2023). Approximately 100 drugs were listed, from which the top five drugs with lowest (strongest) binding ability were selected (Wishart et al. 2018).

Molecular Docking:

AutoDockTools 1.5.7 was used for molecular preparation, Grid box generation to select boundaries of the protein's active zone, marking the ligand anchoring region (Oleg and Arthur J. 2010). The binding pocket details of the protein were mentioned in the system, where the grid point spacing of 1 Å with dimension of 20*18*20 and centre of -9.107, 1.195, 20.101 was used to locate the predicted pocket (generated through DrugRep) for docking. After acquiring the protein and ligand files, the docking was performed using the AutoDock Vina application (Trott and Olson 2010).

Visualization of the docking:

The visualization was done using python-based program system, Pymol (DeLano 2020). The program helps better visualization through high graphics of the structural image and proper binding information of the ligand and protein. The program has several functions like superimposition of several 3-D structures for comparative study, mutation of the mature amino acid residue in the structure and also for sequence structure analysis. The resulting AutoDock Vina output files of both the protein and ligands were used in the Pymol to visualise the area of interaction between them, providing information about the interaction of amino acid residue and ligand. The 3-D image of the interaction was observed and the residue of the protein interacting with ligand was noted down for each of the top five ligands.

RESULTS AND DISCUSSIONS:

Protein Structure Modelling:

The sequence of the protein Cdc37 was acquired and used to retrieve the 3-D model of the protein from Swiss Model. The server provided us with 4 different possible model structure having GMQE score of each. Model_01 showed the highest GMQE score of 0.8 using template Q8X1E6.1.A, Model_02 had a GMQE score of 0.39 using template of 7z38.1.D, Model_03 had GMQE score of 0.04 using template 7xx5.1.U and Model_04 had GMQE score of 0.02 using template 4fq0.1.B. Model_01 was chosen for further validation and docking as the GMQE score of it is near 1.0(Figure 2.2)

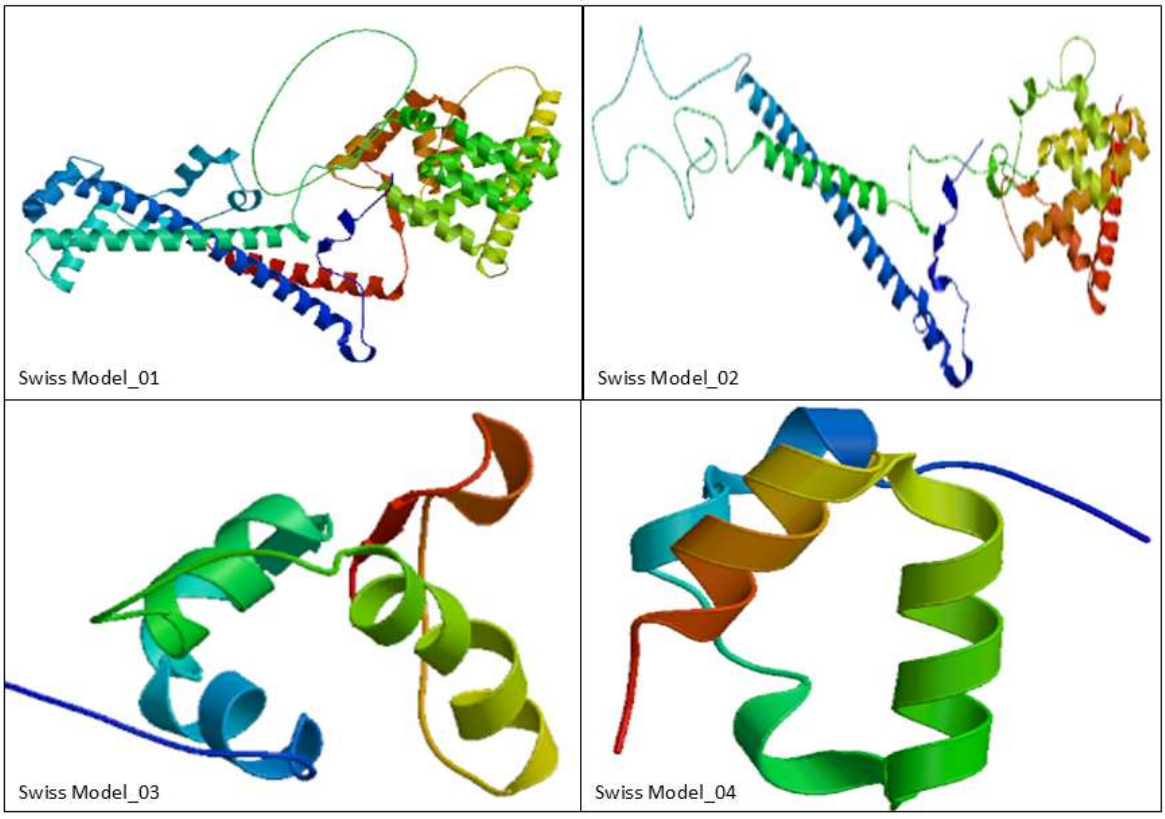

Figure 2.2: Model Structure of Cdc37

Structure Validation:

Saves v6.0 validated the Cdc37 protein structure across four evaluation programs. The ERRAT server provided that the overall quality factor of the protein model is 95.4654, which showed that the quality of the structure obtained from the Swiss Model is preferable to work with [Figure 2.2(A)]. The result of VERIFY3D showed that 55.9% of the residues have an average 3D-1D score >=0.1 [Figure 2.2(B)]. WHATCHECK evaluated 47 structural criteria: 27 passed (green), 13 raised warnings (yellow), and 7 failed. Further clarification was done by PROCHECK server, which provided the Ramachandran Plot, [Figure 2.2(C)]. The plot analysed that 437 (91.8%) of non-glycine and non-proline residues were located in the most favoured regions [A, B, L], while 33 residues (6.9%) were present in the additional allowed regions [a, b, l, p]. A very less proportion of 4 residues (0.8%) occurred in the generously allowed regions and only 2 residues (0.4%) were found in the disallowed regions. As the model has more than 90% of the residues in the most favoured regions, it demonstrated a good stereochemical quality and a comprehensive structural reliability.

The Z-score of ProSA is -9.05, which showed that the overall quality of the protein is good as more negative value represents that the protein is highly native and favourable [Figure 2.2(D)]. The energy plot is also provided along with the Z-score, showing the local model quality through plotting energies as the function of amino acids sequence position [Figure 2.2(E)].

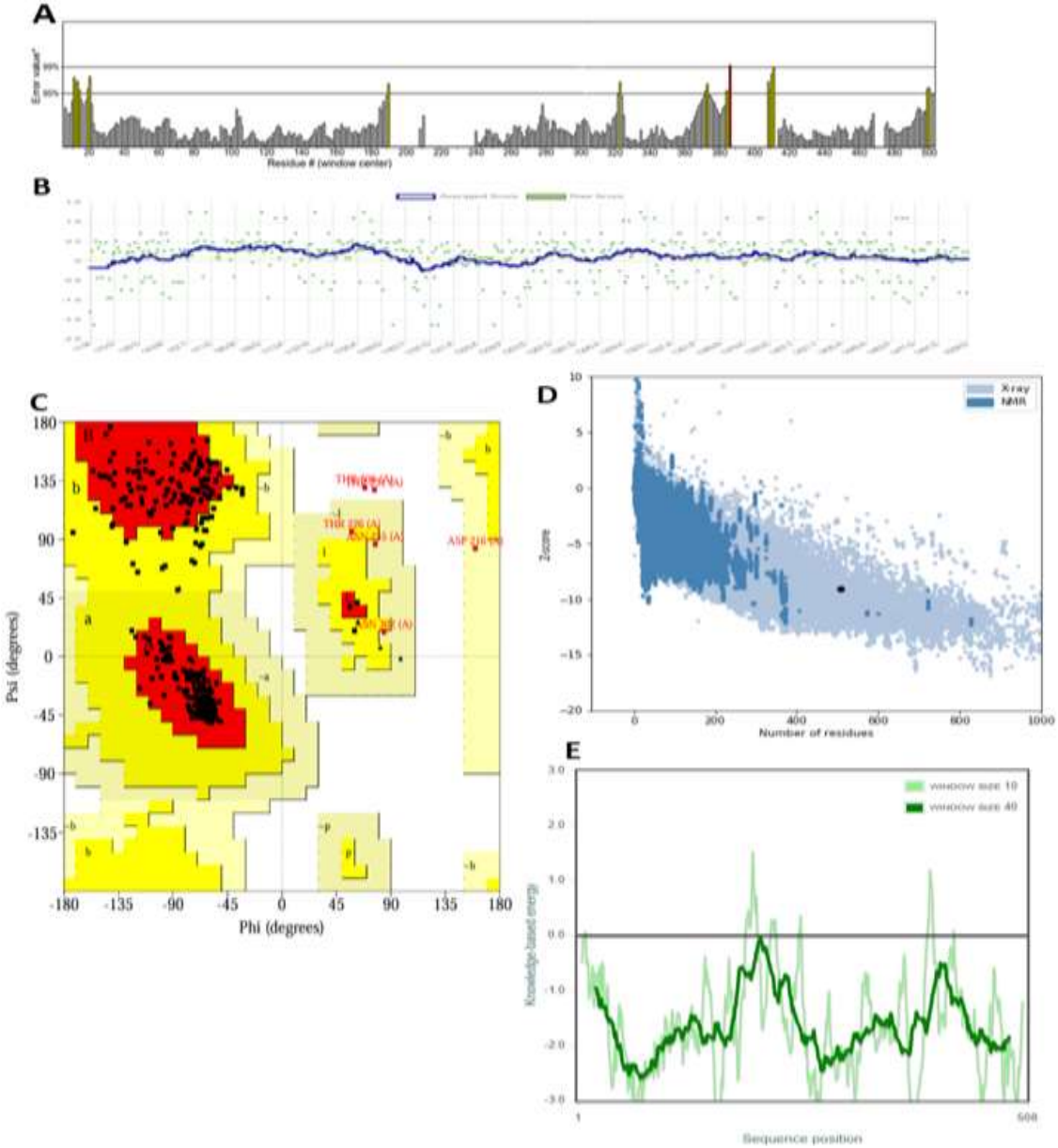

Figure 2.2: (A) Model_01 ERRAT plot showed residues that lacked atom-atom and non-bonded interaction of Cdc37 protein. (B) Model_01 VERIFY3D shows that the 3-D structure of the model matches with the sequence

of the amino acids. (C) Model_01 PROCHECK results gave a Ramachandran plot for the model structure. (D) Model_01 ProSA result is a plot of z-score vs number of residues. (E) Model_01 ProSA result is an energy plot for the protein model structure.

Drug-based Screening:

The DrugRep server predicted the five different pockets of the model protein [Table 3.3(A)]. Each pocket of the protein contains different range of amino acids and pick a suitable pocket that corresponds to the binding site, namely, the N-terminal domain of Cdc37 [Table 3.3(B)]. Each pocket has its own center coordinates and dimensions. The amino acids which are found in the N-terminal domain of Cdc37 from 1-130 residues is our main area of focus. Among the five pockets, the first one was chosen as it contains all the required amino acid residue for the protein kinase interaction (Figure 2.3) and this particular pocket served as a binding site for the drugs. This pocket was used for drug screening, by using FDA approved drug library to avoid ADMET test. 100 drugs were shortlisted from the server. The screened drugs were ranked by their binding affinity scores, and top five compounds with the lowest (most favourable) binding energies were selected for further molecular docking studies [Table 3.3(C)].

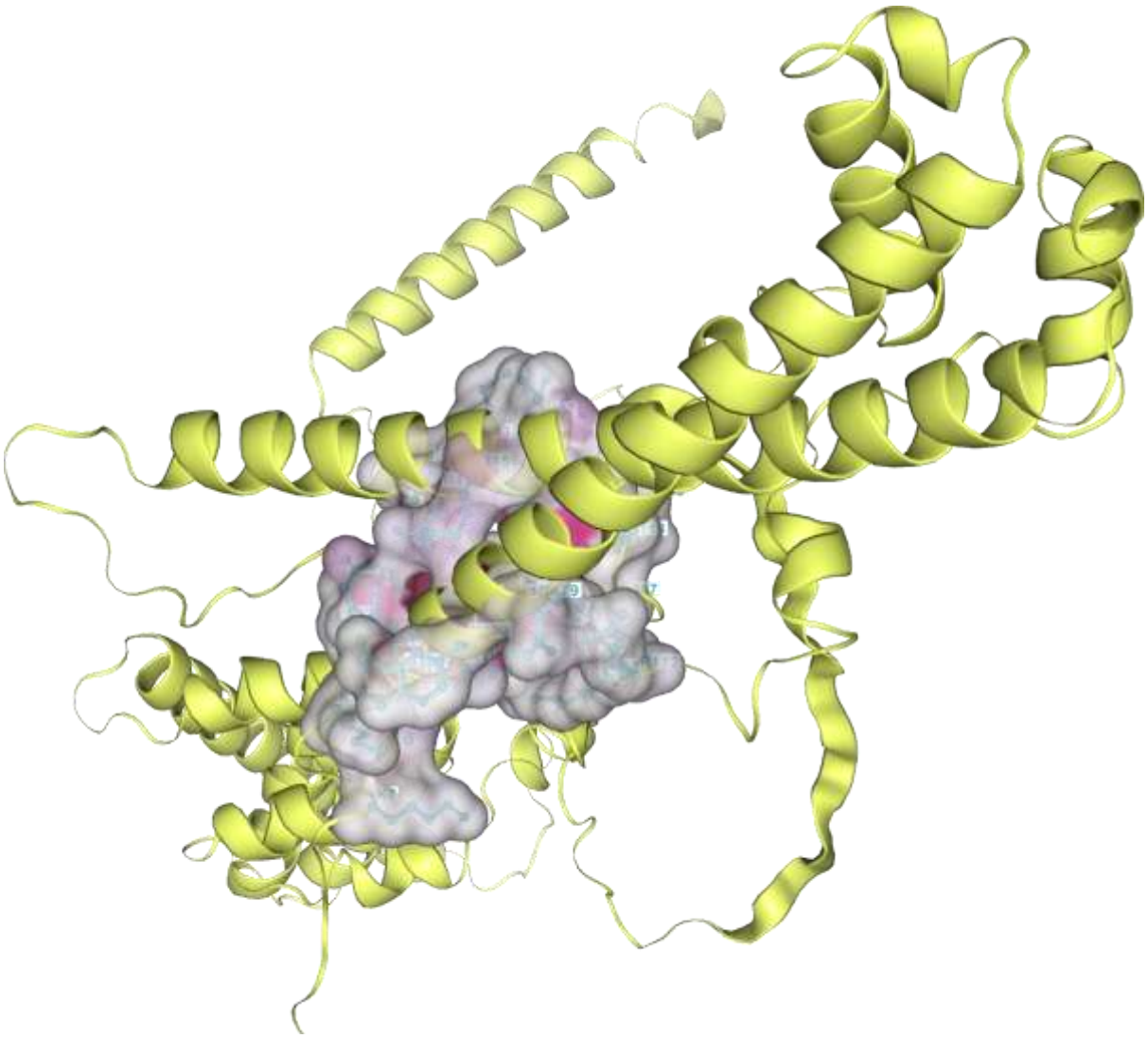

Figure 2.3: Model_01 pocket 1 of Cdc37

Table 3.3(A): The volume, centre and size of all pockets of the model protein are mentioned from the DrupRep server.

POCKET	VOLUME	CENTRE	SIZE
POCKET 01	1057	(-9.1), 1.1, 20.1	20,18,20

POCKET 02	285	(-26.8), 9.9, 17.6	17,13,17
POCKET 03	203	35.5, 18.9, (-35.4)	14,12,10
POCKET 04	142	25.5, (-1.2), (-34.4)	13,10,12
POCKET 05	135	24.0, 29.1, (-72.9)	13,12,11

Table 3.3(B): The five pockets of the model protein structure have different chains of amino acids.

POCKET_01	Chain A (ALA186 LYS113 ARG45 LYS119 ARG42 MET43 ARG112 ASN46 GLY114 LEU118 SER191 ASP192 ASP193 ILE47 ASP179 GLU12 ASP117 LYS185 TYR183 LYS7 LYS10 HSD39 ILE189 LEU182 VAL190 LEU188 LYS50 GLN187)
POCKET_02	Chain A (LYS102 TYR100 PHE120 PHE98 LYS119 GLU126 ARG122 LYS97 LEU103 THR57 ILE125 GLN95 TYR131 ASP99 GLU96 LEU118 LYS61 ASP101)
POCKET_03	Chain A (THR294 LEU298 GLU306 ALA262 LEU291 ILE310 LYS263 LYS259 HSD309 ILE254)
POCKET_04	Chain A (LEU340 ALA352 GLN322 TYR319 LYS344 PHE356 PHE341 ALA355 ILE345 LEU323)
POCKET_05	Chain A (LYS452 ALA396 ILE453 LEU397 LEU451 GLU395 GLU454)

Table 3.3(C): Enlistment of the first five drugs acquired from the DrugRep server according to their screening affinity score. The information of the drugs is also provided including, chemical class, disease targeting and the mode of action.

ID	NAME	SCREENING AFFINITY SCORE (Kcal/mol)	CHEMICAL CLASS	DISEASE TREATING OR MANAGING	Mechanism of action
DB04868	Nilotinib	-9.8	Benzene and substituted derivatives	Chronic Myeloid Leukemia (CML)	Tyrosine kinase inhibitor; Mast/stem cell growth factor receptor KIT inhibitor
DB04869	Venetoclax	-9.6	Carboxylic acids and derivatives	Chronic Lymphocytic Leukemia (CLL), Acute Myeloid Leukemia (AML)	Calcitonin gene-related peptide type 1 receptor
DB04870	Eltrombopag	-9.4	Steroids and steroid derivatives	Promotes body fat loss while maintaining body protein storage, maintaining nitrogen balance	Weight loss through brain "weight thermostat" and body "inhibit white fat storage"
DB04871	Lidoflazine	-8.8	Benzazepines	Management of Obesity	Selective activation of 5-HT2C receptors in the anorexigenic pro-opiomelanocortin neurons in the arcuate nucleus of the hypothalamus; decreased food intake and satiety by promoting the release of alpha-melanocortin

					stimulating hormone, which acts on melanocortin-4 receptors.
DB04872	Regorafenib	-8.8	Benzene and substituted derivatives	Schizophrenia and other Central Nervous System (CNS) disorders	Antagonist activity on Neuromedin-K receptor

Molecular docking and visualization:

The molecular docking calculations performed via AutoDock Vina yielded binding affinities across the top five FDA-approved candidate drugs. Nilotinib exhibited the strongest binding affinity with a score of -9.5kcal/mol (ranging to -8.3 kcal/mol) and formed 2 polar interactions. Eltrombopag demonstrated a binding score ranging from -9.4 kcal/mol to -7.8 kcal/mol with 3 polar interactions. Regorafenib (DB08896) exhibited docking scores between -8.9 kcal/mol and -7.6 kcal/mol with 3 polar interactions. Lidoflazine showed binding affinities between -8.8 kcal/mol and -7.1 kcal/mol with 2 polar interactions. Finally, Venetoclax displayed binding energies ranging from -8.5 kcal/mol to -6.6 kcal/mol with 2 polar interactions.

Visualization of the docking:

The result of the docking-based output files was visualised in the Pymol. The result 3-D visualized the polar interaction between the protein and drugs. These help to map the particular protein residues that bind to different ligand residues [Figure 2.5(a), (b), (c), (d) and (e)]. Visualization in PyMOL revealed the specific amino acid interactions and polar bond distances within Pocket 1 of Model_01. **Nilotinib (DB04868),** interacted with ASP117 and ASP193 at bond distances of 3.4 and 2.6 Å, respectively. **Venetoclax (DB11581),** bound to LYS113 and ASP192 with hydrogen bond distances of 2.6 and 3.2 Å, respectively. **Eltrombopag (DB06210),** formed three polar interactions involving ASP193 (two interaction sites at 3.2 and 2.4 Å) and LYS185 at 2.6 Å. **Lidoflazine (DB13766),** engaged ASP117 at 1.8 Å and ASN46 at 2.1 Å. **Regorafenib (DB08896),** formed three polar connections targeting ASP193 at 2.8 Å and LYS119 across two interaction sites at 2.3 and 2.5 Å.

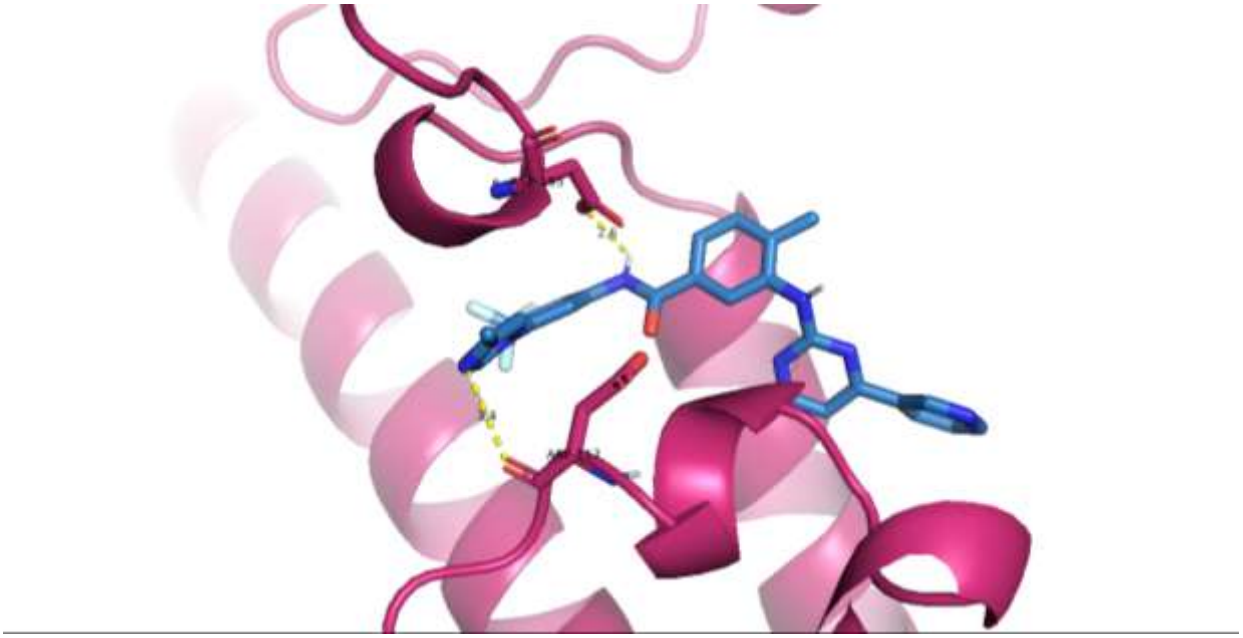

Figure 2.5(a): The protein Cdc37 and the ligand with, Nilotinib interaction. The ligand is bound to the protein through two polar bonds.

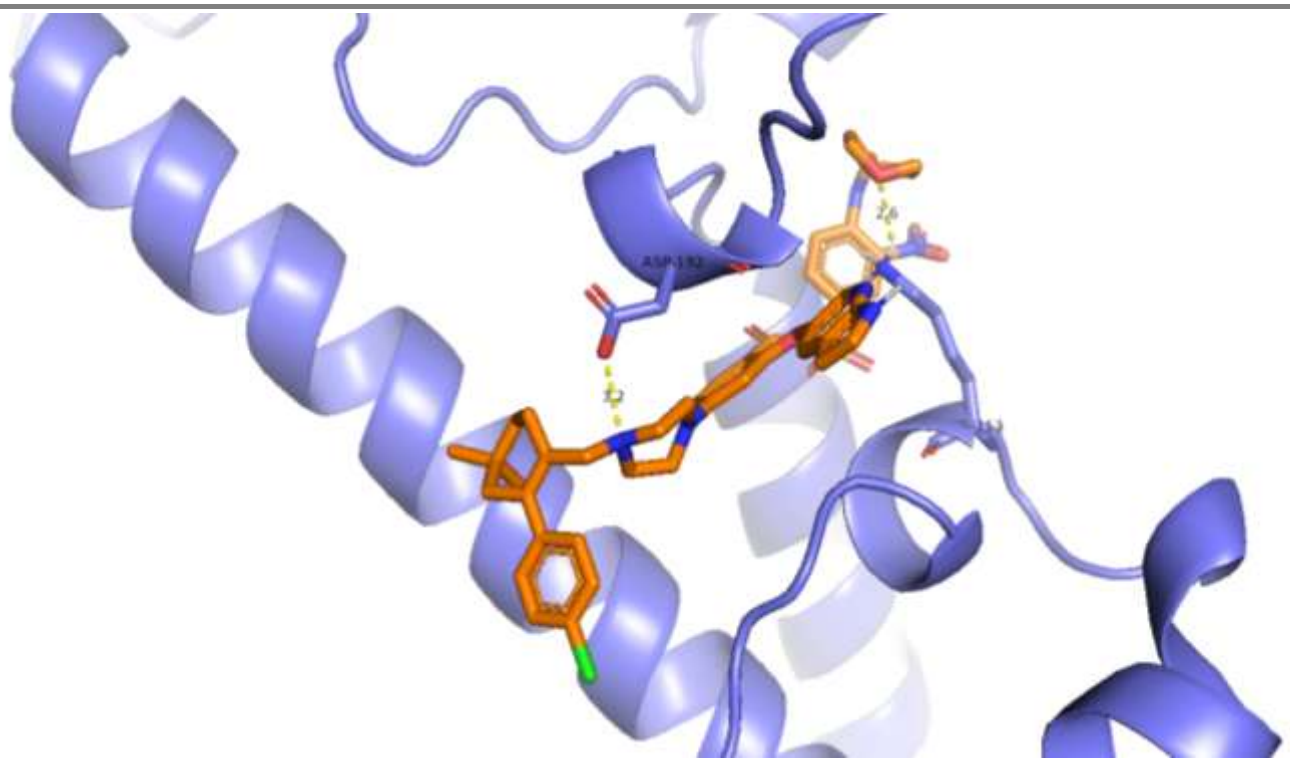

Figure 2.5(b): The protein Cdc37 and the ligand Venetoclax interaction. The ligand binds to the protein through polar bonds in two positions.

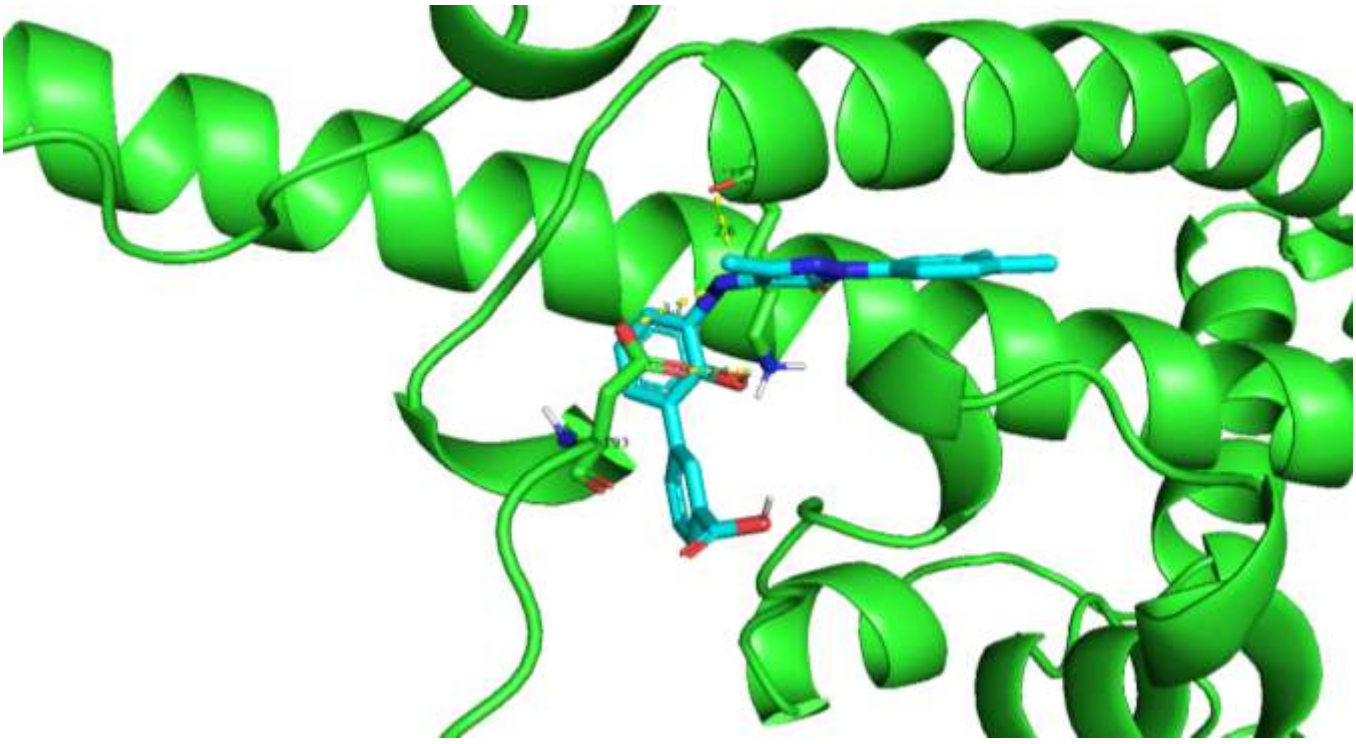

Figure 2.5(c): The protein Cdc37 and the ligand, Eltrombopag interaction. The ligand binds to the protein through polar bonds in two positions with three interaction sites on the ligand binding at one position.

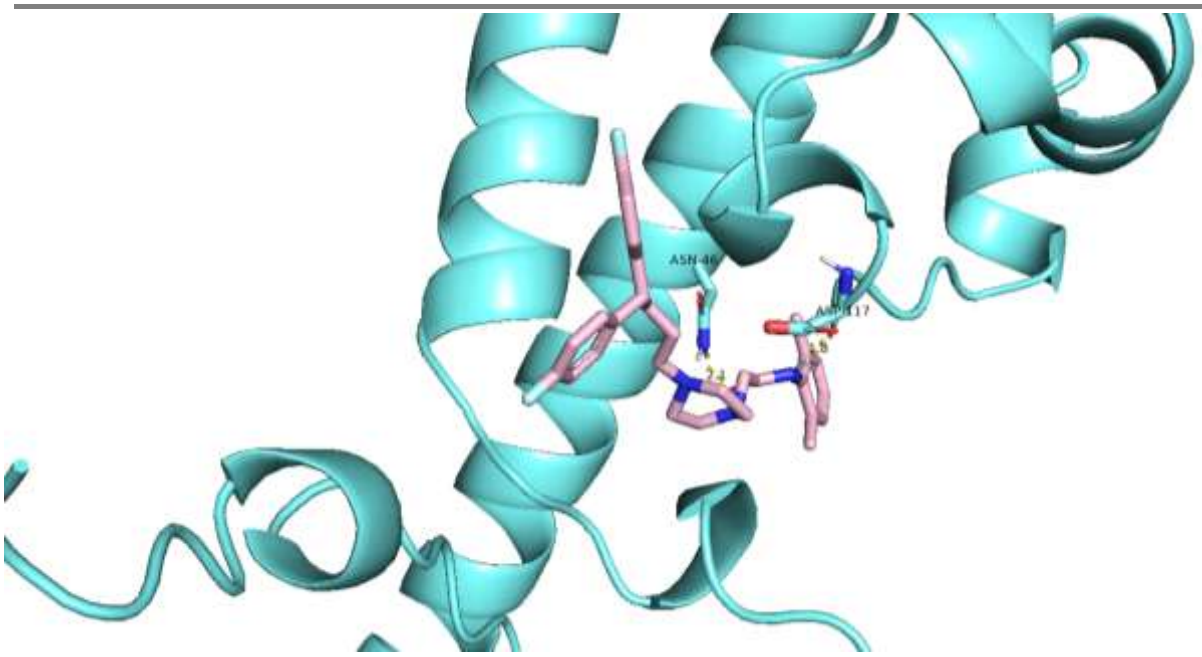

Figure 2.5(d): The protein Cdc37 and the ligand, Lidoflazine interactions. The ligand binds to the protein through polar bonds in two positions.

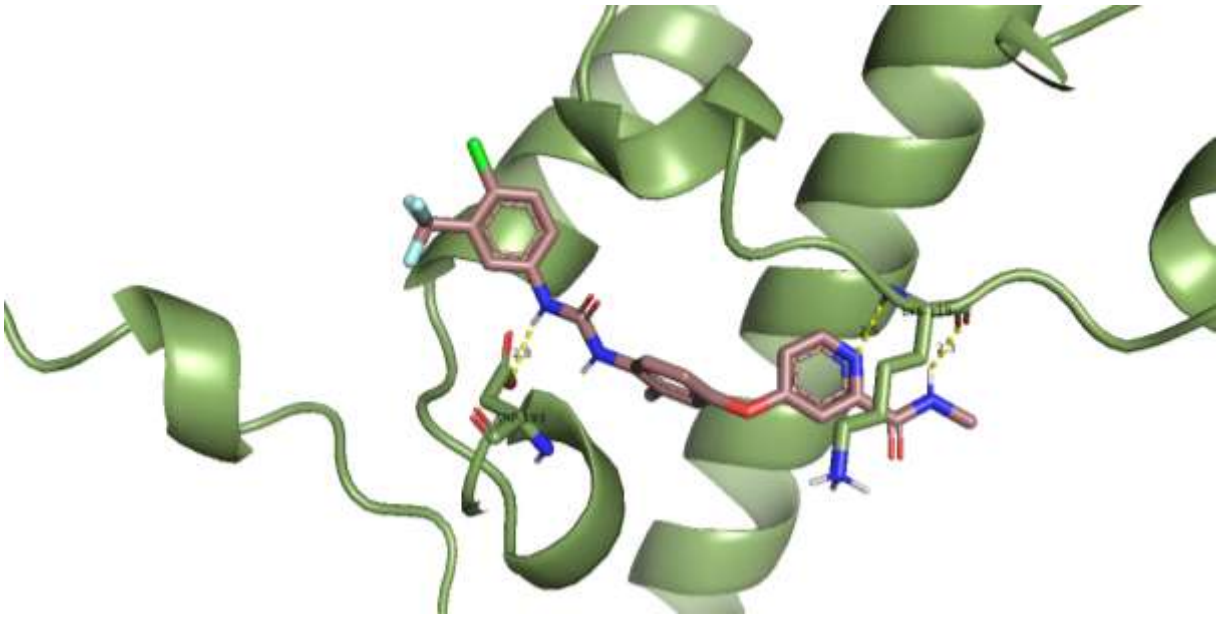

Figure 2.5(e): Model_01, the green coloured structure represents the protein, Cdc37 and the brown colour structure shows the ligand with ID- DB08896. The ligand binds to the protein at two positions with three interaction sites on the ligand.

CONCLUSION:

This study identified potential target inhibitors that bind to the N-terminal region of Cdc37 to disrupt its interaction with Pkc1. The drug that proved to bind the best and inhibit the interaction is Nilotinib with Drug ID- DB04868. Furthermore, the computational homology model demonstrated favourable stereochemical quality and favourable binding energy for the virtual docking. The drug Nilotinib is a tyrosine kinase inhibitor itself, so the kinase catalytic activity domain recognizes the Cdc37 N-terminal domain, thereby resisting the interactions of Pkc1 kinase binding activity. Tyrosine-protein kinase acts as a cell-surface receptor for the cytokine KITLG/SCF and performs an essential function in cell survival and proliferation regulation, hematopoiesis, stem cell maintenance, gametogenesis, mast cell development, migration and function, and in melanogenesis. Disrupting this interaction within the Pkc1 domain may reduce hyphal growth and subsequently

impair biofilm formation. Further studies can be done on the direct interaction of Pkc1-Cdc37, a structural visualization of the complex and protein-protein virtual docking to study the pathway involved before Hsp90 interaction with the binary complex. Additionally, further computational research into Pkc1 involvement in morphogenesis is warranted, as current structural and mechanistic data remain limited.

ACKNOWLEDGEMENTS

TS would like to acknowledge the Faculty Research Grant and RUSA Grant at University of Kalyani for the funding necessary for the research work.

Declaration of competing interest

The Authors declare no conflicts of interest

REFERENCE

1. **Bateman, A., Martin, M. J., Orchard, S., Magrane, M., Ahmad, S., Alpi, E., ... & UniProt Consortium.** (2023). UniProt: the Universal Protein Knowledgebase in 2023. *Nucleic Acids Research*, 51(D1), D523–D531. https://doi.org/10.1093/nar/gkac1052
2. **Biasini, M., Bienert, S., Waterhouse, A., Arnold, K., Studer, G., Schmidt, T., ... & Schwede, T.** (2014). SWISS-MODEL: Modelling protein tertiary and quaternary structure using evolutionary information. *Nucleic Acids Research*, 42(W1), W252–W258. https://doi.org/10.1093/nar/gku340
3. **Ciurea, C. N., Kosovski, I. B., Mare, A. D., Toma, F., Pintea-Simon, I. A., & Man, A.** (2020). *Candida* and candidiasis—opportunism versus pathogenicity: a review of the virulence traits. *Microorganisms*, 8(6), 857. https://doi.org/10.3390/microorganisms8060857
4. **DeLano, W. L.** (2020). *The PyMOL Molecular Graphics System* (Version 2.3). Schrödinger, LLC.
5. **Diezmann, S., Michaut, M., Shapiro, R. S., Bader, G. D., & Cowen, L. E.** (2012). Mapping the Hsp90 genetic interaction network in *Candida albicans* reveals environmental contingency and rewired circuitry. *PLoS Genetics*, 8(3), e1002562. https://doi.org/10.1371/journal.pgen.1002562
6. **Engler, S., Delhommel, F., Dodt, C., Lopez, A., Faust, O., Elimelech, A., ... & Buchner, J.** (2026). The essential co-chaperone Sgt1 regulates client dwell time in the Hsp90 chaperone cycle. *Molecular Cell*, 86(2), 166–179. https://doi.org/10.1016/j.molcel.2025.12.002
7. **Gan, J. H., Liu, J. X., Liu, Y., Chen, S. W., Dai, W. T., Xiao, Z. X., & Cao, Y.** (2023). DrugRep: an automatic virtual screening server for drug repurposing. *Acta Pharmacologica Sinica*, 44(4), 888–896. https://doi.org/10.1038/s41401-022-00996-2
8. **Ghannoum, M. A., Jurevic, R. J., Mukherjee, P. K., Cui, F., Sikaroodi, M., Naqvi, A., & Gillevet, P. M.** (2010). Characterization of the oral fungal microbiome (mycobiome) in healthy individuals. *PLoS Pathogens*, 6(1), e1000713. https://doi.org/10.1371/journal.ppat.1000713
9. **Keramisanou, D., Aboalroub, A., Zhang, Z., Liu, W., Marshall, D., Diviney, A., ... & Gelis, I.** (2016). Molecular mechanism of protein kinase recognition and sorting by the Hsp90 kinome-specific cochaperone Cdc37. *Molecular Cell*, 62(2), 260–271. https://doi.org/10.1016/j.molcel.2016.04.005
10. **Mayer, F. L., Wilson, D., & Hube, B.** (2013). *Candida albicans* pathogenicity mechanisms. *Virulence*, 4(2), 119–128. https://doi.org/10.4161/viru.22913
11. **Nobile, C. J., & Johnson, A. D.** (2015). *Candida albicans* biofilms and human disease. *Annual Review of Microbiology*, 69, 71–92. https://doi.org/10.1146/annurev-micro-091014-104330
12. **Robbins, N., & Cowen, L. E.** (2023). Roles of Hsp90 in *Candida albicans* morphogenesis and virulence. *Current Opinion in Microbiology*, 75, 102345. https://doi.org/10.1016/j.mib.2023.102351
13. **Spampinato, C., & Leonardi, D.** (2013). *Candida* infections, causes, targets, and resistance mechanisms: traditional and alternative antifungal agents. *BioMed Research International*, 2013, 204237. https://doi.org/10.1155/2013/204237
14. **Sudbery, P. E.** (2011). Growth of *Candida albicans* hyphae. *Nature Reviews Microbiology*, 9(10), 737–748. https://doi.org/10.1038/nrmicro2636

15. **Trott, O., & Olson, A. J.** (2010). AutoDock Vina: improving the speed and accuracy of docking with a new scoring function, efficient optimization, and multithreading. *Journal of Computational Chemistry*, 31(2), 455–461. https://doi.org/10.1002/jcc.21334
16. **Tsui, C., Kong, E. F., & Jabra-Rizk, M. A.** (2016). Pathogenesis of *Candida albicans* biofilm. *Pathogens and Disease*, 74(4), ftw018. https://doi.org/10.1093/femspd/ftw018
17. **Waterhouse, A., Bertoni, M., Bienert, S., Studer, G., Tauriello, G., Gumienny, R., ... & Schwede, T.** (2018). SWISS-MODEL: Homology modelling of protein structures and complexes. *Nucleic Acids Research*, 46(W1), W296–W303. https://doi.org/10.1093/nar/gky427
18. **Wiederstein, M., & Sippl, M. J.** (2007). ProSA-web: Interactive web service for the recognition of errors in three-dimensional structures of proteins. *Nucleic Acids Research*, 35(suppl_2), W575–W576. https://doi.org/10.1093/nar/gkm290
19. **Wishart, D. S., Feunang, Y. D., Guo, A. C., Lo, E. J., Marcu, A., Grant, J. R., ... & Knox, C.** (2018). DrugBank 5.0: A major update to the DrugBank database for 2018. *Nucleic Acids Research*, 46(D1), D1074–D1082. https://doi.org/10.1093/nar/gkx1037
20. **Xie, J. L., Grahl, N., Sless, T., Leach, M. D., & Cowen, L. E.** (2016). Signaling through Lrg1, Rho1 and Pkc1 governs *Candida albicans* morphogenesis in response to diverse cues. *PLoS Genetics*, 12(11), e1006405. https://doi.org/10.1371/journal.pgen.1006405